ANAS Transactions **Earth Sciences** **2 / 2023**

http://www.journalesgia.com

THE IMPACT OF COULOMB STRESS CHANGES OF THE 2018 M_w7.5 PALU EARTHQUAKE, INDONESIA

Ahadov B.[1,2], Jin Sh.[3,4]

[1]Ministry of Science and Education of the Republic of Azerbaijan,
Institute of Geology and Geophysics, Azerbaijan
119 H. Javid ave., Baku, AZ1143: ahadovshao@gmail.com
[2]Ministry of Science and Education of the Republic of Azerbaijan,
Institute of Oil and Gas, Azerbaijan
9, F.Amirov ave., Baku, AZ 1000
[3]Shanghai Astronomical Observatory, Chinese Academy of Sciences
80 Nandan Road, Shanghai 200030, China
[4]School of Surveying and Land Information Engineering,
Henan Polytechnic University, Jiaozuo 454000, China

Keywords: *Coulomb stress, stress inversion, deformation, earthquake, Palu, Indonesia*

Summary. This paper studied the effects of Coulomb stress in understanding the proximity to failure on the Palu-Koro fault system. An earthquake occurred on a large strike-slip fault in the northern part of Sulawesi Island, Indonesia, on September 28, 2018. Coulomb stress increased by approximately 1 bar, corresponding closely to the locations of aftershocks and areas where stress dropped by more than 10 bars. Based on the focal mechanisms of the aftershocks and source models of the main shock, the Coulomb failure stress changes on both of the focal mechanism nodal planes are calculated. Additionally, we calculated the changes in Coulomb stress on the focal sources of each aftershock. Our stress model indicates a positive correlation within the areas of the extended Coulomb stress caused by the combination of seismic activities. We investigated the Coulomb stress as a possible origin for the aftershocks, which are most likely to slip optimally oriented for failure due to the local stress field generated by the mainshock. The Palu 7.5 earthquake led to the distribution of surface displacements. Moreover, calculated horizontal displacement increased in the NW-SW direction, ranging from 1 to 1.3 meters. The stress maps included in this paper are crucial in predicting the expected locations of future aftershocks and mitigating the potential for earthquakes.

Introduction

Shallow earthquakes frequently exert destructive effects on nearby communities. Historically, this region has witnessed numerous large earthquakes with a magnitude of 6 and above, and extensive ruptures spanning over 250 km throughout the past century. Notably, the largest earthquake took place on January 1996, ~ 100 km north of the earthquake that occurred on September 28, 2018. This 1996 earthquake transpired in the regional subduction zone at a shallow depth causing fatalities, substantial property damage, and numerous injuries in the surrounding area (Source: USGS). It's essential to acknowledge that central Sulawesi has been recording earthquakes since the 18th century. Many of these seismic events were catastrophic and were followed by tsunamis. Historically, Palu Bay witnessed a significant seismic event in 1927 that released a huge tsunami with a height of 15 m. In a similar event nearly seven decades later, Donggala was struck in 1996 by a tsunami with wave heights ranging between 1-3 m.

On September 28, 2018, a moment magnitude 7.5 earthquake struck the northern region of Palu, Sulawesi (Fig. 1). The mainshock occurred at a shallow depth on the Palu-Koro fault located within the interior of the Molucca microplate on the Sunda tectonic plate. The earthquake's focal mechanism solution indicates that it was caused by a strike-slip on

faults trending both north-south and west-east. This seismic event took place on the Palu-Koro fault with an approximate rupture length of 150 km. The earthquake resulted in significant damage to buildings and infrastructure leading to thousands of fatalities and even more injuries. The aftermath of this event included ground shaking, landslides, and a tsunami, all contributing to the catastrophic impact.

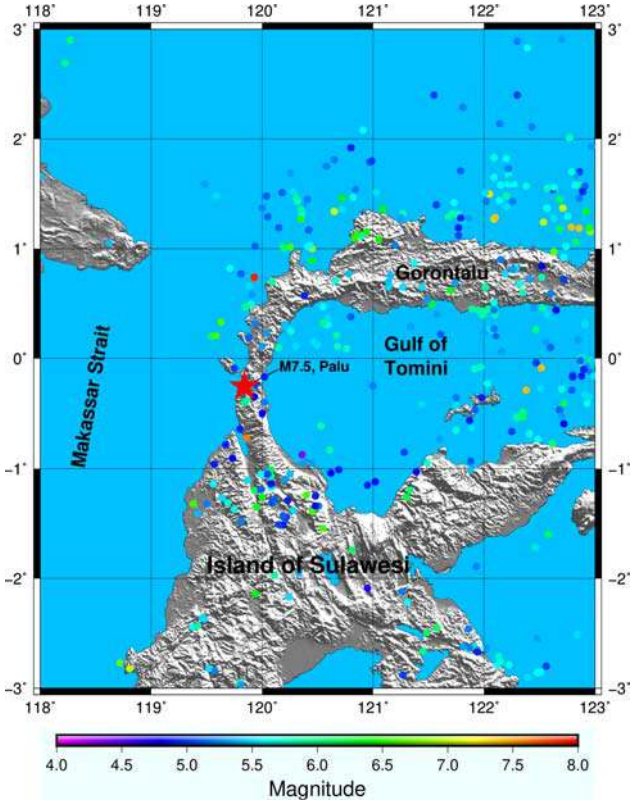

Fig. 1. Simplified topographic map of the study area. Highlighted dots are earthquakes $M_w \geq 4$ seismicity from ISC (1976-2018)

The concept of static Coulomb stress changes, induced by a primary earthquake, can potentially trigger subsequent earthquakes along neighbouring faults. Therefore, changes in earthquake stress can be employed in the evaluation of potential seismic hazards (King et al., 1994; Ahadov, Jin, 2019). The stress change and its effects associated with the Loma Prieta, California shock have been the subject of numerous studies (Lin, Stein, 2004; Reasenberg and Simpson, 1992). Hardebeck et al., (1998) applied the Coulomb stress transfer model to examine the impacts of the Landers and Northridge earthquakes. However, comparing co-seismic stress changes with earthquakes represents a significant oversimplification of the complex natural processes involved in earthquake triggering. Coulomb stress changes induced by the main shock are evaluated by calculating the stress variations across both optimally oriented and specific fault planes. The results from these calculations suggest that there is no clear evidence that the Coulomb stress changes created by the main shock facilitated the occurrence of the aftershocks.

We analyzed the correlation between components of the comprehensive Coulomb failure stress to understand the process of earthquake triggering accurately. We utilized stress interaction methods to determine how the earthquake affected the potential for failure along the Palu-Koro fault. These findings are applied to assess the acceleration or delay of future earthquakes in Palu, Sulawesi.

Tectonic Setting

Sulawesi Island is located among the Philippine, Australian, and Sunda plates and surrounds the continental convergence sections of the Sunda margin. The triple junction in Southeast Asia is highly seismically active and is characterized by active rotations of small blocks reported by both geological and kinematic studies (Kreemer et al., 2000; Silver, Moore, 1978; Simons et al., 2000; Stevens et al., 1999; Walpersdorf et al., 1998) (Fig. 2). The main active structures in Sulawesi are the Palu-Koro fault and its south-eastern extension to Matano. The Palu-Koro fault divides the islands into two blocks: the North Sula Block to the northeast and the Makassar Block to the southwest (Fig. 2). GPS and block modelling data suggest a slip rate of 42 mm/year in the area of the Palu-Koro fault (Socquet et al., 2006). A significant active structure on land in the west of Central Sulawesi is the NW-SE trending Palu-Koro strike-slip fault, which forms the boundary between the Makassar and North Sula blocks (Kreemer et al., 2000). The slip velocity on this fault is estimated to be within the range of 30-40 mm per year (Bellier et al., 2001). Certain parallel fault strands determine the margins of a pull-apart basin in Palu.

The Australian and Philippine plates are subducting beneath the Sunda plate at rates between 75-90 mm/year (Socquet et al., 2006). The W-E trending plate boundary zone extending from the New Guinea Trench to East Indonesia, establishes the relative motion between the Pacific and Australian plates via block rotations and transgression faulting (Tregoning et al., 2000; Wallace et al., 2004). The subduction of the Australian plate beneath the Sunda plate occurs at the Sunda-Banda Arc. The Java Trench extends from the collision in Australia to approximately 600 km south of Sulawesi. Specifically, the southwestern part of Sulawesi rotates counter-clockwise in relation to the Sunda Plate, while the North Sula Block and the northeastern Manado Block rotate clockwise towards the NNW.

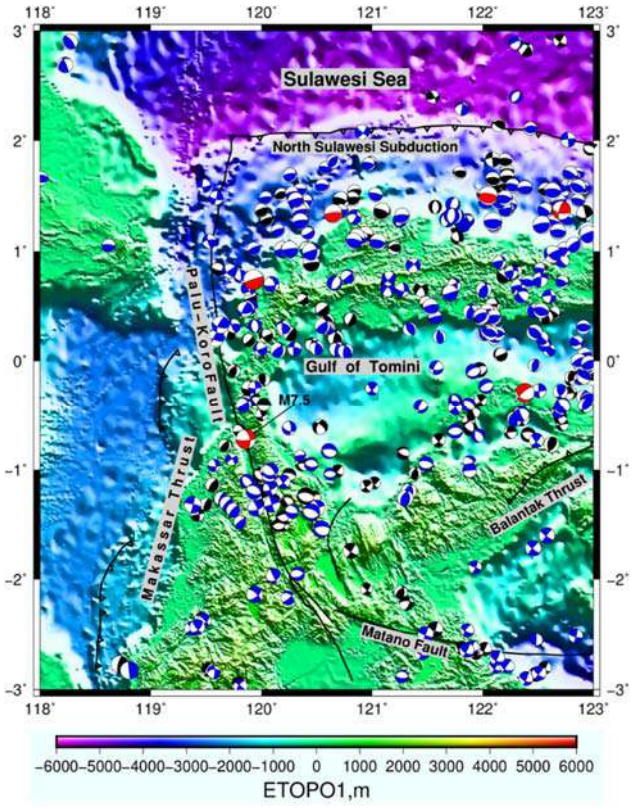

Fig. 2. Simplified topographic/bathymetric and tectonic setting map of the study area. Major active tectonic structures and faults are shown. The focal mechanism solutions are from the Global Centroid Moment Tensor (GCMT, black) and International Seismological Centre (ISC, blue) catalogs. Red balls are $M_w \geq 7$, 1976-2019.

Method

Coulomb Failure

While statistical seismology often provides probabilities for aftershock locations and timings, accurate prospective earthquake predictions demand a physical understanding of earthquake distribution. Comprehending how static stress accumulates over time through tectonic plate movement or co-seismic and post-seismic slip may serve as a foundation for determining earthquake probabilities over timeframes that extend beyond typical aftershock duration periods (Strader, 2014).

Variations in the Coulomb failure stress due to the mainshock are resolved onto the fault plane of the affected earthquake using strike, dip, and rake angles in the stress calculations. Future failure areas have been identified by the increased effects of the Coulomb stress.

$$\Delta\sigma_f = \Delta\tau - \mu'\Delta\sigma_n \qquad (1)$$

where $\Delta\tau$ and $\Delta\sigma_n$ are the change in normal and shear stresses on likely future fault planes. The effective coefficient of friction denoted as μ takes into account the effects of changes in pore pressure and typically ranges from 0 to 0.8 (Roeloffs, 1988). The confining stress can be related to fluid pore pressure by Skempton's coefficient, B, which quantifies the ratio of the change in pore pressure in a cavity to the change in applied stress. The Coulomb stress is contingent on the accuracy of the initial earthquake parameters. Minor variations in fault geometry and slip distribution can lead to significant alterations in Coulomb failure stress.

We used Coulomb 3.4 software (Lin and Stein, 2004; Toda et al., 2005) to compute the co-seismic static stress changes resulting from the magnitude 7.5 Palu earthquake on optimally oriented faults. In our model, the Earth was presumed to be a homogenous elastic half-space, and faults were treated as rectangular dislocations. To accommodate these assumptions, we considered values for Young's modulus, shear modulus, and Poisson's ratio were considered as $8x10^5$ bar, $3.2x10^5$ bar, and 0.25, respectively. We utilized an empirically value of 0.4 and 0.6 for the effective friction coefficient (μ'). To estimate the average slip for an earthquake, we applied empirical relationships from Wells and Coppersmith (1994) which correlate event rupture length, width, magnitude, and surface displacement.

Stress Inversion

The stress variations have been projected onto the optimally oriented mainshock strike-slip, thrust, and normal faults using the regional stress field defined in this study. The stress inversion method developed by Michael (1984) provided definitions for normal and shear stresses on a fault σ_n and:

$$\sigma_n = T_i n_i = \tau_{ij} n_i n_j \qquad (2)$$

$$\tau N_i = T_i - \sigma_n n_i = \tau_{ij} n_j - \tau_{jk} n_j n_k n_i = \\ = \tau_{kj} n_j \left(\delta_{jk} - n_i n_k\right) \qquad (3)$$

where δ_{ik} is the Kronecker delta, T is the traction along the fault, n is the fault normal and N is the unit direction vector of shear stress along the fault. Afterwards, equation (3) is revised as follows:

$$\tau_{kj} n_j (\delta_{ik} - n_i n_k) = \tau N_i \, . \qquad (4)$$

Michael (1984) employed the Wallace-Bott theory and defined the shear stress direction denoted as N with the slip direction s of shear movement along the fault. He further proposed that the shear stress τ on active faults maintains a consistent ratio across all studied earthquakes. Subsequently, equation (4) is represented in matrix form:

$$At = s \qquad (5)$$

where t represents the vector of stress components.

$$t = [\tau_{11}\tau_{12}\tau_{13}\tau_{22}\tau_{23}]^T \quad (6)$$

A is the 3 × 5 matrix calculated from fault normal n,

$$\begin{bmatrix} n_1(n_2^2+2n_3^2) & n_2(-n_1^2+n_3^2) & n_3(-2n_1^2-n_2^2) \\ n_2(1-2n_1^2) & n_1(1-2n_2^2) & -2n_1n_2n_3 \\ n_3(1-2n_1^2) & -2n_1n_2n_3 & n_1(1-2n_3^2) \\ n_1(-n_2^2+n_3^2) & n_2(n_1^2+2n_3^2) & n_3(-n_1^2-2n_2^2) \\ -2n_1n_2n_3 & n_3(1-2n_1^2) & n_2(1-2n_3^2) \end{bmatrix}^{\mathbf{T}} \quad (7)$$

The degree of correlation hinges on several factors: the precision of source/receiver hypocentre locations and focal mechanism parameters, as well as physical source characteristics. Michael's algorithm employs both nodal planes to try to identify the exact fault planes while determining the optimal stress tensor. A key feature of the algorithm is the calculation of the confidence limits of the principal stress axes directions, which is performed through a statistical method known as bootstrap resampling. The algorithm seeks to minimize the discrepancy between the slip direction and the projected tangential traction while maintaining a consistent and significant magnitude of tangential traction across various fault planes. Although it is somewhat conjectural, the use of a simple fracture criterion suggests keeping the tangential traction similar from one fault plane to another. This fracture criterion further implies that the isotropic component of the stress tensor dominated the normal traction on the fault planes.

Results and Discussion

Local stress inversion

Over the past 30 years, it has been widely accepted that the location and timing of recurring earthquakes (aftershocks) are largely influenced by stress changes resulting from displacement due to the main shock. Interest in the issue of the effect of stress changes on subsequent seismic activity was triggered following minor events 17 years before the 1992 earthquake near Landers, California (USA) with M 7.4 led to a stress increase at the epicentre and along the majority of the future rupture line (Stein et al., 1992). Furthermore, the majority of aftershocks occurred in the area where an increase in stress was observed. Multiple studies have since discovered a quantitative correlation between static voltage changes and the location of subsequent major shocks and aftershocks (Harris, 1998; Steacy et al., 2005; King, 2007; Hardebeck, Okada, 2018).

Alterations in Coulomb stress are derived from displacements associated with corresponding earthquakes. These displacements induce perturbations in the stress tensor within the fault, potentially leading to both shear and normal components. An increase in shear stress, contemporary with the displacement direction, and a decrease in normal stress collectively enhance the probability of future failure.

Numerous methods have been proposed to determine tectonic stress from earthquake focal mechanism solutions. The most commonly used methods were developed by Michael (1984) and Gephart and Forsyth (1984). These methods typically assume that tectonic stress is homogeneous within the region, that earthquakes occur on pre-existing faults with varying orientations, and that the slip vector aligns with the shear stress direction on the fault. In this study, we have used Focal Mechanism Solutions (FMS) from Harvard CMT (Ekström et al., 2012) and International Seismological Centre (ISC, http://www.isc.ac.uk) for our region of interest (Fig. 2).

Michael (1984) proposed determining the stress that minimizes the discrepancy between the resolved shear stress and the slip direction for each dataset. These algorithms outline the directions of the three principal stress axes, as well as the relative magnitudes of these stress axes. In this context, $\sigma1$, $\sigma2$, and $\sigma3$ indicate the maximum, intermediate, and minimum principal compressive stresses, respectively.

The defining feature of the stress field is its utility in outlining deformation zones and active tectonic structures at local and regional levels. We created two distinct datasets of focal mechanisms, one from GCMT and another from ISC to assess the capability of stress ratio R under varying stress conditions. We performed stress inversion on these fault planes using the same process developed by Vavryčuk (2014). The R-values for all zones fall within the range of 0.3 to 0.7 indicating that the magnitude of the intermediate principal stress ($\sigma2$) is relatively close to midway between the magnitudes of the $\sigma1$ and $\sigma3$ axes (when $R = 0.5$). The inversion results demonstrate that the maximum principal stress ($\sigma1$) is oriented in the NW-SE direction while the minimum stress axis ($\sigma3$) strikes in the NE-SW direction and is sub-vertical. The intermediate principal stress ($\sigma2$) is trending sub-horizontal for the Palu region (refer to Table, Fig. 3).

Comparison of stress tensor inversion results for the region

Region	σ_1(tr)	σ_1(pl)	σ_2(tr)	σ_2(pl)	σ_3(tr)	σ_3(pl)	Phi (R)
Palu	293.6	35.5	114.6	54.4	24	0.5	0.51±0.03

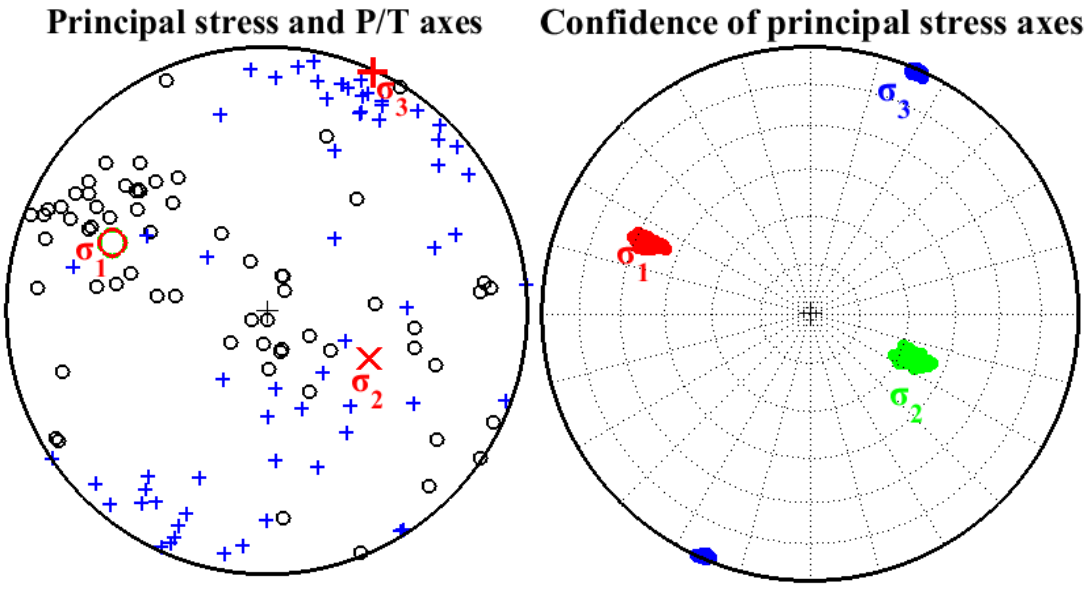

Fig. 3. The map represents the P and T axes of the focal mechanisms and dots delineate the distribution of the stress axis within the 95% confidence range. Azimuth (Az) and plunge (Pl)

Coulomb stress

We studied the Coulomb stress hypothesis for the 2018 Palu earthquake in Indonesia using focal mechanism solutions as receiver faults in the Coulomb stress pattern. The correlation between the Coulomb stress and seismic activity generated by the Palu event and preceding incidents suggests regions at risk for significant future events. The main shock was preceded by foreshocks starting about three hours earlier with an event located south of the epicenter. The Coulomb stress patterns were calculated at a depth of 10 km due to the main shock.

The stress model depicts four distinct lobes of increased Coulomb stress and four lobes of Coulomb stress reduction (Fig.4). The extended lobes are located at the end of the fault, while the regions of decreased Coulomb stress host the other lobes. The distribution of aftershocks aligns with these patterns. A Coulomb stress change of less than 1 bar is sufficient to trigger events, while the same amount can effectively suppress them (King et al., 1994). The largest lobe of the decreased Coulomb stress is centered on the epicenter of the rupture plane, where stresses dropped by approximately 11 bars. The stresses generated by earthquake slip can cause fracturing, and the resulting stress increases can lead to further earthquakes. Most of the aftershocks have occurred in areas where the Coulomb failure stress has increased by ≥ 1 bar, and a significant number of aftershocks are located where the stress has decreased in the E-S direction (Fig. 4).

Coulomb stress models are calculated on an optimally oriented fault plane using local stress results. The calculation results of the optimum orientations and Coulomb stress changes are presented in Figure 4 (b, c, and d). Negative Coulomb stress changes dominate within the rupture area, while positive stress changes are observed in the northwest and southeast parts of the rupture. In the case of normal faulting orientation (Fig. 4d), most of the aftershocks concentrate in the area of positive stress change, except for a few earthquakes in the rupture zone where negative stress changes were observed. The lobed models of stress variation using local stress adjustments encompass large areas of negative change that dominate towards landward and offshore of the main rupture with positive stress changes occurring in the SW-NE direction inland and offshore in the case of an optimum thrust faulting (Fig. 4c).

The vertical cross-section confirms that the fault plane is associated with the mainshock (Fig.5). The aftershocks occur in regions of negative stress changes and some are located in areas of positive stress changes. The vertical cross-sections provide extended data on the stress distribution in strike-slip faulting situations as seen in Figure 5. The study of the stress produced on a cross-section reveals that the Coulomb stress increase occurs in the areas where aftershocks were located at different depths. It can be seen that the region towards C-C' is more likely to have aftershocks due to increased stress accumulation. There are possibilities that the aftershocks might have propagated towards the south, and the most probable direction is towards the southeast.

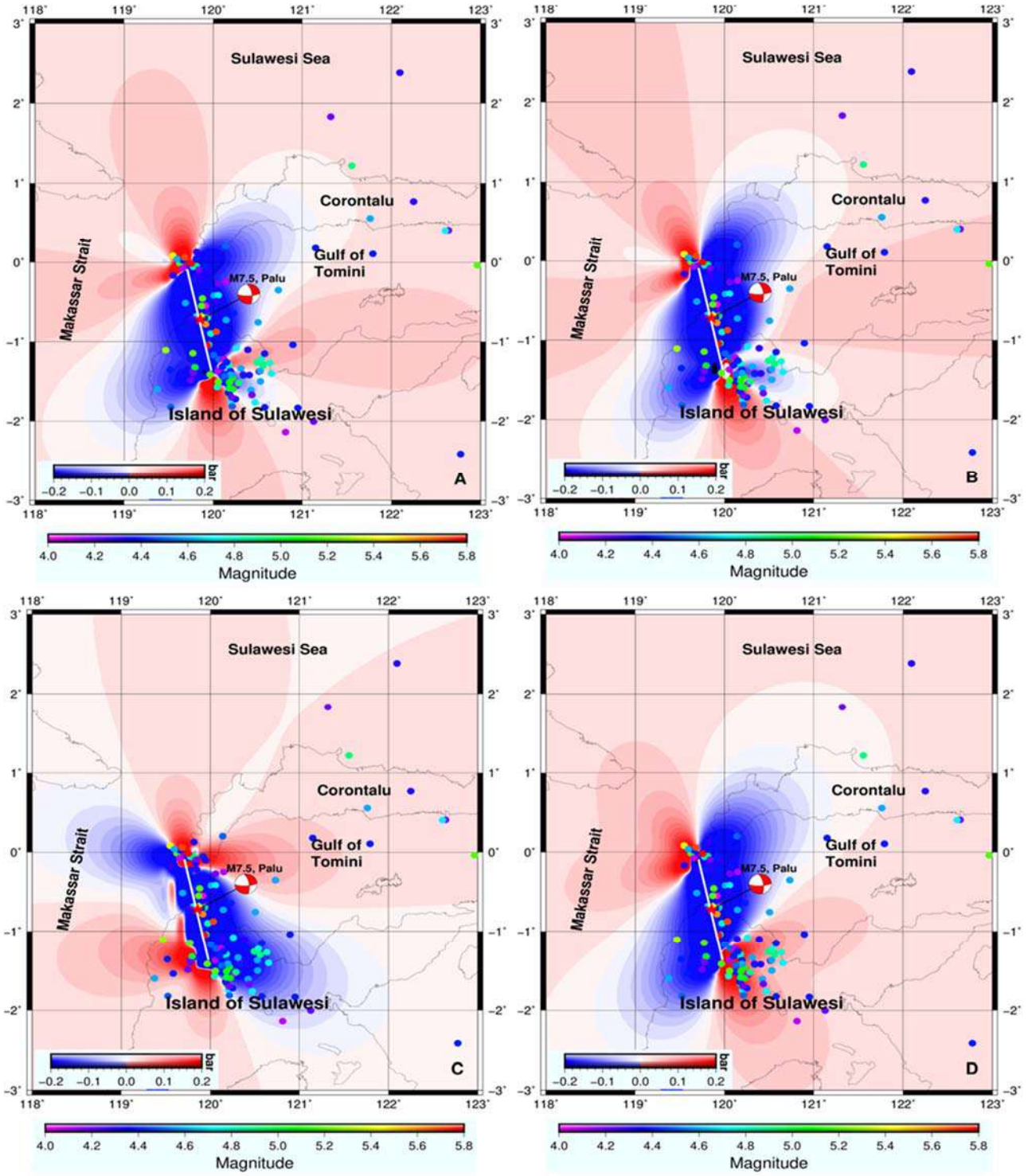

Fig. 4. Map shows Coulomb stress changes caused by the 2018 Palu earthquake calculated over the optimally oriented (a) strike 348^0; dip 57^0; rake -15^0 (gCMT) (b) strike-slip faulting (c) thrust faulting and (d) normal faulting. The highlighted dots denote the epicenters of the $M \geq 4$ aftershocks (USGS)

The assumed value for effective friction contributes to the calculated Coulomb stress changes, and thus the correspondence of Coulomb stress changes to aftershock distributions. Typically, studies aim to identify the effective coefficient of friction that leads to the best fit of aftershocks using this technique to infer frictional strength. King et al. (1994) found that adjustments to friction only had noticeable effects on aftershock correlations and thus preferred to use the value of 0.4. Moreover, Coulomb stress changes are calculated at different depths and friction values from a finite fault modelling result (USGS, us1000h3p4). The occurrence of several aftershocks in an area of the calculated Coulomb stress decrease may be due to the oversimplification of the fault slip, heterogeneities of crustal characteristics, or orientations of the fault.

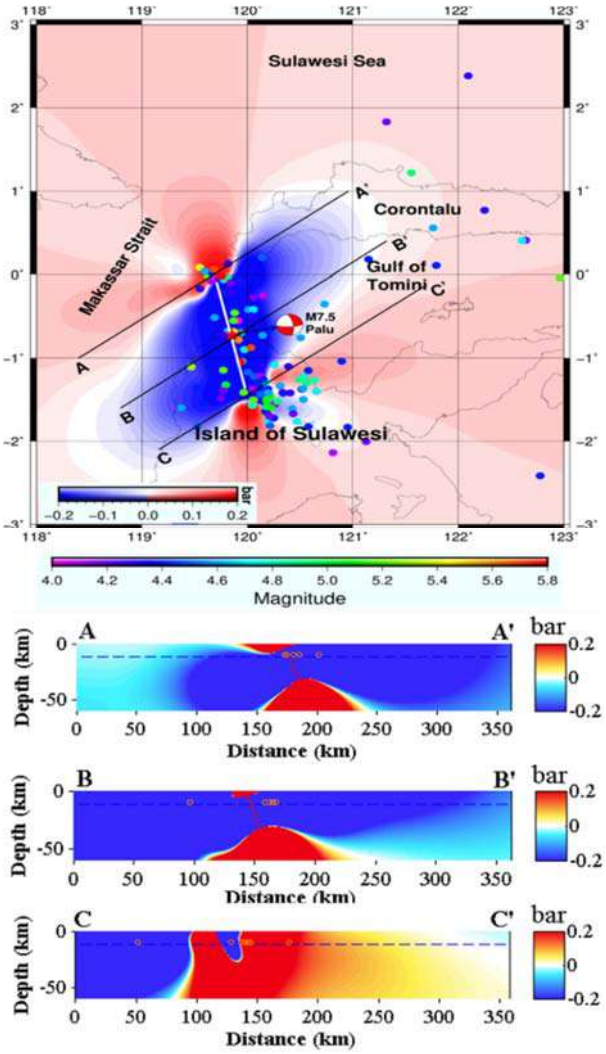

Fig. 5. Vertical cross-sections oriented perpendicular to the strike of the fault modelling during the 2018 Palu earthquake along lines P1 (A-A'), P2 (B-B') and P3 (C-C')

Figure 6 illustrates the effects of static stress when the friction coefficients are at typical values of 0.4 and 0.6. For different values a distinct level of difference is observed in the number of triggered aftershocks when the coefficient is 0.6 at a depth of 15 km, and 30% of the aftershocks occur in the areas of increased stress. The static Coulomb stress triggering effect does not improve significantly with variations in the friction coefficient value. Coseismic Coulomb stress change calculations have effectively described aftershock distributions following the 1995 Kobe, Japan earthquake (Toda et al., 1998), and the 1989 M = 7.1 Loma Prieta earthquake (Reasenberg, Simpson, 1992). The presence of several aftershocks in areas of the decreased Coulomb stress may result from oversimplifications of modeled fault slip or the existence of faults with different orientations. The application of Coulomb stress changes to explain aftershock distributions challenges the long-standing theory that earthquakes occur randomly.

Displacement and Strain rate

Therefore, considering all of the above mentioned, we calculated the average slip distribution from empirical relationships between average slip and magnitude. The earthquake struck the island of Sulawesi, approximately 78 km north of Palu. The earthquake triggered a tsunami that was 4 to 7 m high, which affected the coastal areas of western Sulawesi, including Donggala and the city of Palu. We created a displacement map that reveals vertical and horizontal surface movement across the entire fault. Figure 7 presents the results of calculations of the seismic displacement of the Earth caused by the earthquake. The fault extends to the southeast, and the most substantial horizontal displacement mainly occurs in the NNW and SW parts of the fault. Horizontal displacement in the north-south direction is larger than the displacement in the southwestern direction. The red color indicates positive displacement (elevation), while blue represents negative displacement. This map aids in understanding the type of faulting associated with an earthquake. Figure 8 demonstrates that the rupture from the Palu earthquake has the vertical displacements are approximately 2 m offshore in the NW direction.

The release of strain between events is what triggers earthquakes. In this study, we tried to understand the distribution of strain caused by the Palu earthquake. The strain tensor is calculated concerning six components: three normal and three shear strain components. The normal components of strain are oriented towards the *x, y,* and *z* directions. Figure 8 shows that aftershocks predominantly accumulate negative strain in various directions. However, not only negative strain significant for a future shock, but positive strain changes can also induce future events. A positive change in Coulomb stress in the future could be substantial enough to alter the level of strain on the regional fault, potentially causing rupture. Our analysis determined that the strain maps of the earthquake demonstrate a response that is roughly similar to that of the Coulomb stress indicating the accumulation of strain along the SE direction.

Conclusion

Assessing the Coulomb stress associated with earthquake slip has been confirmed to be an essential means of understanding diverse seismic phenomena. Such calculations have successfully illustrated aftershock distributions, the locations of triggered earthquakes, stress increases at the edges of a ruptured fault, and off-fault lobes of stress increase. Areas of Coulomb stress decrease have also been identified to align with regions of minimal aftershock activity.

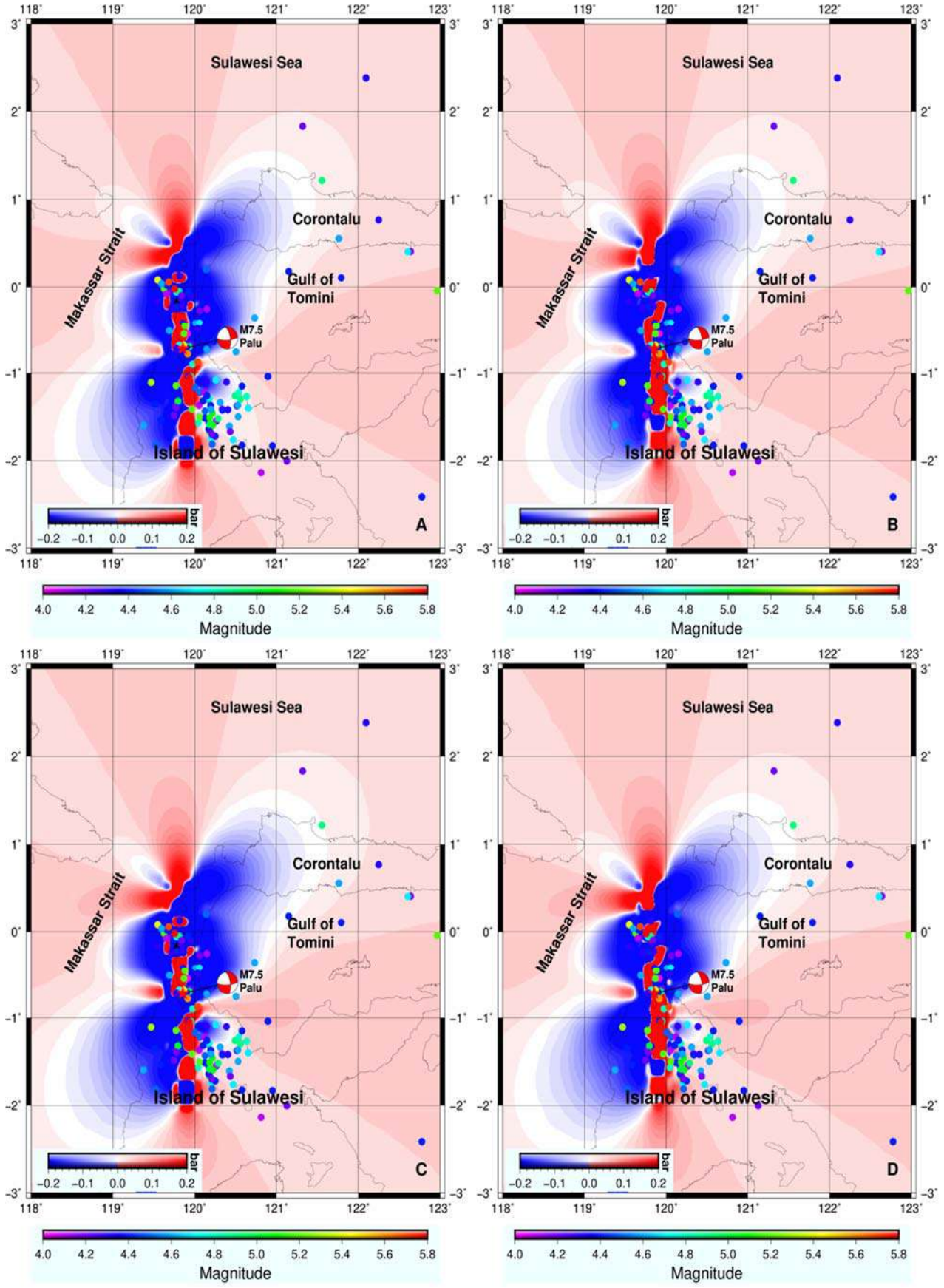

Fig. 6. Illustration of Coulomb stress changes based on Gavin Hayes's finite fault model (USGS/NEIC). (a) Depth: 10 km; μ 0.4, (b) Depth: 15 km; μ 0.4, (c) Depth: 10 km; μ 0.6, (d) Depth: 15 km; μ 0.6

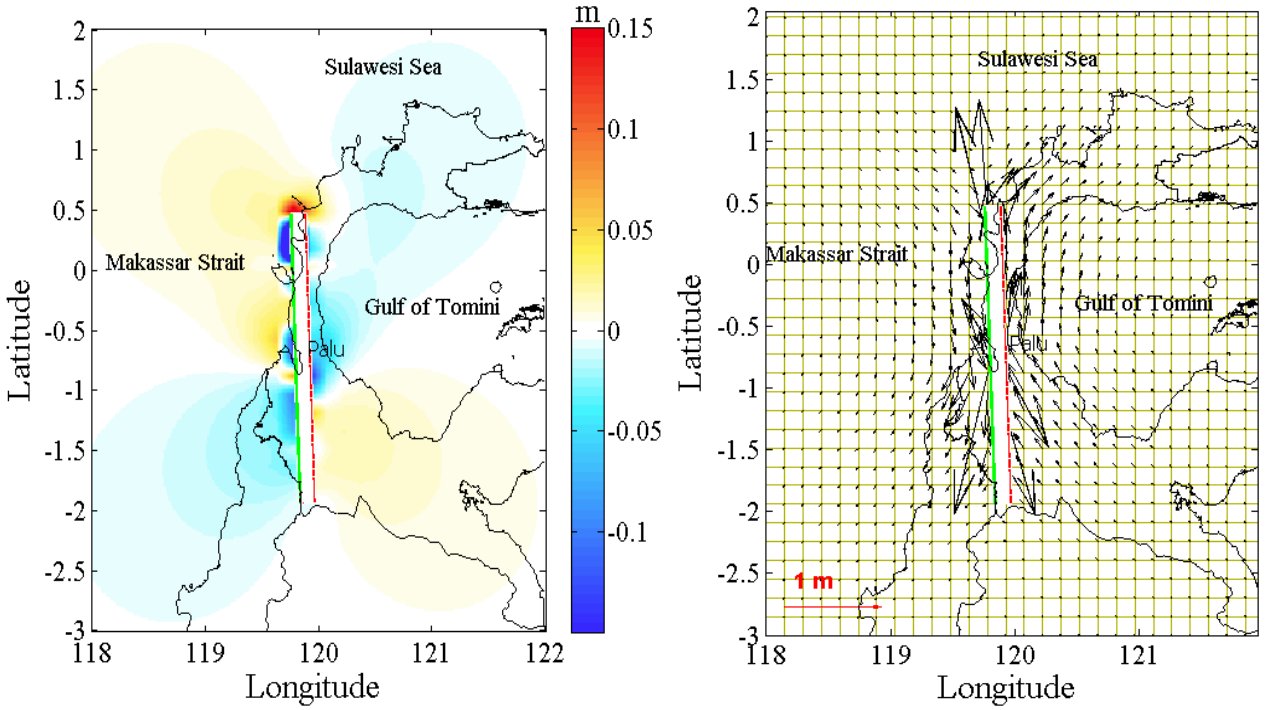

Fig. 7. Horizontal displacement map of the region enclosing the epicenter of the earthquake immediately after the mainshocks (**right**). Vertical cross-sectional view of the displacement of the crust (**left)**

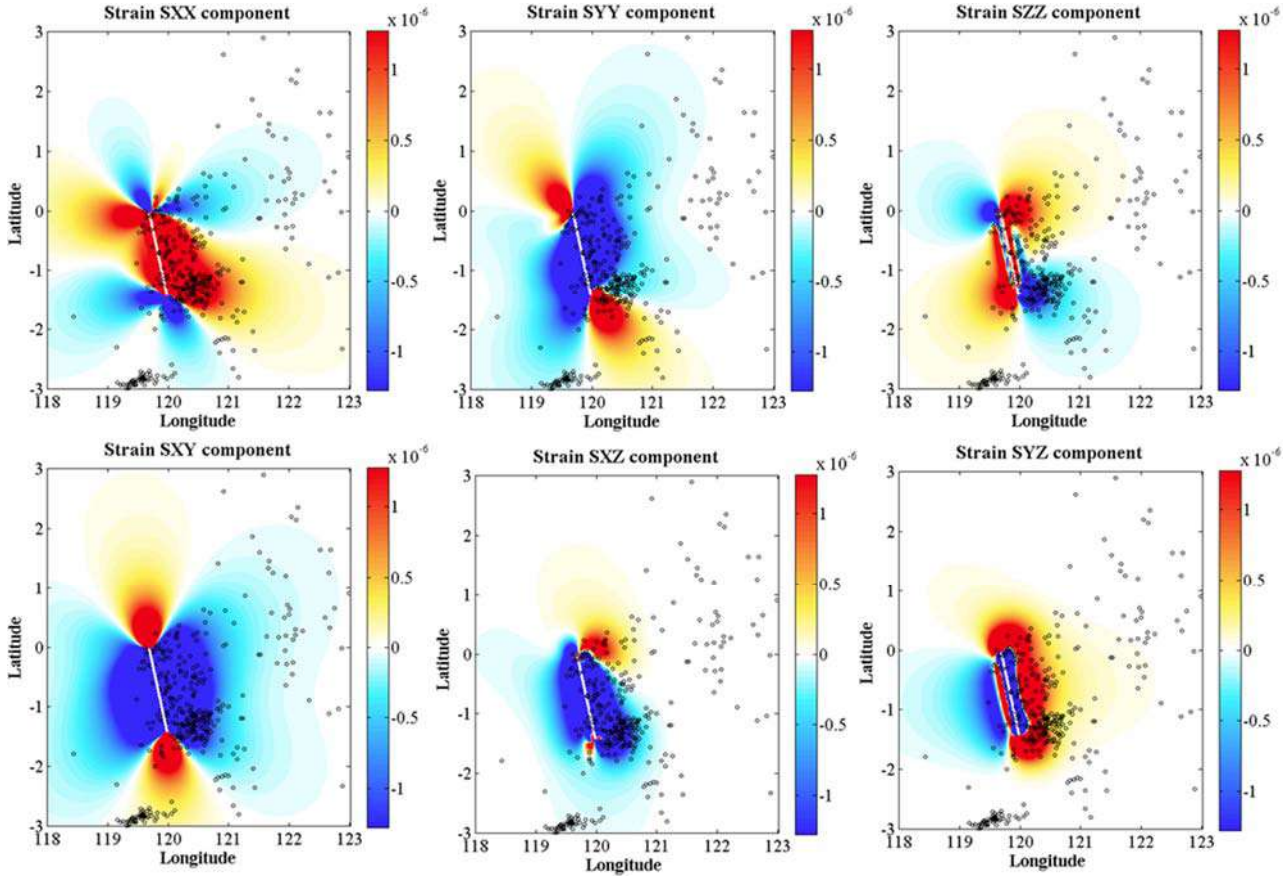

Fig. 8. Normal strain along the x-direction, y-direction, z-direction, and the shear strain in the XY, XZ, and YZ planes of the 2018 Palu earthquake

In this research, we focused exclusively on static stress changes transmitted from the co-seismic fault slips of the main shock. We examined Coulomb stress changes associated with the 2018 Mw7.5 Palu earthquake. The stress model maps demonstrated a correspondence between the main shocks and the observed spatial distribution of aftershocks. These aftershocks were found to be influenced by their relative locations to the rupture plane and source mechanisms, and their dense distribution areas expanded towards the southeast. The stresses transmitted by the Palu earthquake to the adjacent segment of the Palu-Koro fault loaded 1-2 bars of stress at the end of the rupture plane. Stress modelling confirms that minor increases (a few bars) may promote the occurrence of earthquakes. Coulomb stress modelling can serve as a powerful tool for seismic hazard mitigation and aftershock activity prediction. Stress reductions from the earthquake and triggering times are small relative to the recurrence time of the earthquakes.

Acknowledgement

All the maps are drawn using Generic Mapping Tools (GMT) (Wessel et al., 2013).

REFERENCES

Ahadov B., Jin S. Effects of Coulomb stress change on Mw> 6 earthquakes in the Caucasus region. Physics of the Earth and Planetary Interiors, Vol. 297, 106326, 2019, https//doi.org/ 10.1016/ j.pepi.2019.106326.

Bellier O., Sébrier M., Beaudouin T., Villeneuve M., Braucher R., Bourles D., Siame L., Putranto E., Pratomo I. High slip rate for a low seismicity along the Palu-Koro active fault in central Sulawesi (Indonesia). Terra Nova, Vol. 13, No. 4, 2001, pp. 463-470, DOI:10.1046/j.1365-3121.2001.00382.

Ekström G., Nettles M., Dziewoński A. The global CMT project 2004-2010: Centroid-moment tensors for 13,017 earthquakes. Physics of the Earth and Planetary Interiors, Vol. 200-201, 2012, pp. 1-9, DOI: 10.1016/J.pepi.2012.04.002.

Gephart J.W., Forsyth D.W. An improved method for determining the regional stress tensor using earthquake focal mechanism data: application to the San Fernando earthquake sequence. Journal of Geophysical Research: Solid Earth, Vol. 89, 1984, pp. 9305-9320, https://doi.org/10.1029/JB089iB11p09305.

Hardebeck J.L., Nazareth J.J., Hauksson E. The static stress change triggering model: Constraints from two southern California aftershock sequences. Journal of Geophysical Research: Solid Earth, Vol. 103, No. B10, 1998, pp. 24427-24437.

Hardebeck J.L., Okada T. Temporal stress changes caused by earthquakes: A review. Journal of Geophysical Research: Solid Earth, Vol. 123, No. 3-4, 2018, pp. 1350-1365, DOI:10.1002/2017jBO 14617.

Harris R.A. Introduction to special section: Stress triggers, stress shadows, and implications for seismic hazard. J. Geophys. Research., Vol. 103, No. B10, 1998, pp. 24347-24358.

King G.C., Stein R.S., Lin J. Static stress changes and the triggering of earthquakes. Bulletin of the Seismological Society of America, Vol. 84, No. 3, 1994, pp. 935-953.

King G.C.P. Fault interaction, earthquake stress changes, and the evolution of seismicity. Treatise on Geophysics, Vol. 4, 2007, pp. 225-255, DOI:10.1016/B978-044452748-6.00069-9.

Kreemer C., Holt W.E, Goes S., Govers R. Active deformation in eastern Indonesia and the Philippines from GPS and seismicity data. Journal of Geophysical Research: Solid Earth, Vol. 105**,** No. B1, 2000, pp. 663-680.

Lin J., Stein R.S. Stress triggering in thrust and subduction earthquakes and stress interaction between the southern San Andreas and nearby thrust and strike-slip faults. Journal of Geophysical Research: Solid Earth, Vol. 109, No. B2, 2004, 19 p., DOI:org/10.1029/2003JB002607

Michael A.J. Determination of stress from slip data: faults and folds. Journal of Geophysical Research: Solid Earth, Vol. 89, No. B13, 1984, pp. 11517-11526, DOI:10.1029/JBO89i13p11517.

Reasenberg P.A., Simpson R.W. Response of regional seismicity to the static stress change produced by the Loma

ЛИТЕРАТУРА

Ahadov B., Jin S. Effects of Coulomb stress change on Mw> 6 earthquakes in the Caucasus region. Physics of the Earth and Planetary Interiors, Vol. 297, 106326, 2019, https//doi.org/ 10.1016/ j.pepi.2019.106326.

Bellier O., Sébrier M., Beaudouin T., Villeneuve M., Braucher R., Bourles D., Siame L., Putranto E., Pratomo I. High slip rate for a low seismicity along the Palu-Koro active fault in central Sulawesi (Indonesia). Terra Nova, Vol. 13, No. 4, 2001, pp. 463-470, DOI:10.1046/j.1365-3121.2001.00382.

Ekström G., Nettles M., Dziewoński A. The global CMT project 2004-2010: Centroid-moment tensors for 13,017 earthquakes. Physics of the Earth and Planetary Interiors, Vol. 200-201, 2012, pp. 1-9, DOI: 10.1016/J.pepi.2012.04.002.

Gephart J.W., Forsyth D.W. An improved method for determining the regional stress tensor using earthquake focal mechanism data: application to the San Fernando earthquake sequence. Journal of Geophysical Research: Solid Earth, Vol. 89, 1984, pp. 9305-9320, https://doi.org/10.1029/JB089iB11p09305.

Hardebeck J.L., Nazareth J.J., Hauksson E. The static stress change triggering model: Constraints from two southern California aftershock sequences. Journal of Geophysical Research: Solid Earth, Vol. 103, No. B10, 1998, pp. 24427-24437.

Hardebeck J.L., Okada T. Temporal stress changes caused by earthquakes: A review. Journal of Geophysical Research: Solid Earth, Vol. 123, No. 3-4, 2018, pp. 1350-1365, DOI:10.1002/2017jBO 14617.

Harris R.A. Introduction to special section: Stress triggers, stress shadows, and implications for seismic hazard. J. Geophys. Research., Vol. 103, No. B10, 1998, pp. 24347-24358.

King G.C., Stein R.S., Lin J. Static stress changes and the triggering of earthquakes. Bulletin of the Seismological Society of America, Vol. 84, No. 3, 1994, pp. 935-953.

King G.C.P. Fault interaction, earthquake stress changes, and the evolution of seismicity. Treatise on Geophysics, Vol. 4, 2007, pp. 225-255, DOI:10.1016/B978-044452748-6.00069-9.

Kreemer C., Holt W.E, Goes S., Govers R. Active deformation in eastern Indonesia and the Philippines from GPS and seismicity data. Journal of Geophysical Research: Solid Earth, Vol. 105**,** No. B1, 2000, pp. 663-680.

Lin J., Stein R.S. Stress triggering in thrust and subduction earthquakes and stress interaction between the southern San Andreas and nearby thrust and strike-slip faults. Journal of Geophysical Research: Solid Earth, Vol. 109, No. B2, 2004, 19 p., DOI:org/10.1029/2003JB002607

Michael A.J. Determination of stress from slip data: faults and folds. Journal of Geophysical Research: Solid Earth, Vol. 89, No. B13, 1984, pp. 11517-11526, DOI:10.1029/JBO89i13p11517.

Reasenberg P.A., Simpson R.W. Response of regional seismicity to the static stress change produced by the Loma

Prieta earthquake. Science, Vol. 255, No. 5052, 1992, pp. 1687-1690, DOI:10.1126/science 255.5052.1687.

Roeloffs E.A. Hydrologic precursors to earthquakes: A review. Pure and applied geophysics, Vol. 126, 1988, pp. 177-209.

Silver E.A., Moore J.C. The Molucca sea collision zone, Indonesia. Journal of Geophysical Research: Solid Earth, Vol. 83, 1978, pp. 1681-1691.

Simons W., van Loon D., Waspersdorf A., Ambrosius B., Kahar J., Abidin H., Sarsito D., Vigny C., Abu S.H., Morgan P. Geodynamics of SE Asia: First results of the Sulawesi 1998 GPS campaign. In: Geodesy Beyond 2000, Springer. 2000, pp. 271-277.

Socquet A., Simons W., Vigny C., McCaffrey R., Subarya C., Sarsito D., Ambrosius B., Spakman W. Microblock rotations and fault coupling in SE Asia triple junction (Sulawesi, Indonesia) from GPS and earthquake slip vector data. Journal of Geophysical Research: Solid Earth,Vol. 111, No. B8, 2006, DOI: org/10.1029JBOO3963.

Stevens C., McCaffrey R., Bock Y., Genrich J., Subarya C., Puntodewo S. and Vigny C. Rapid rotations about a vertical axis in a collisional setting revealed by the Palu fault, Sulawesi, Indonesia. Geophysical Research Letters, Vol. 26, No. 17, 1999, pp. 2677-2680, DOI:org/10.1029/1999GE008344.

Strader A.E. The effects of Coulomb stress change on Southern California earthquake forecasting. UCLA. ProQuest ID: Strader_ucla_0031D_12803. Merritt ID: ark:/13030/m58d22pj, 2014,166 , DOI:10.13140/RG.22.36576.48647.

Steacy S., Nalbant S.S., McCloskey J., Nostro C., Scotti O., Baumont D. Onto what planes should Coulomb stress perturbations be resolved? J. Geophys. Res., Vol. 110, No. B5, 2005, B05S15, DOI: 10.1029/2004JBOO3356.

Stein R.S., King G.C.P., Lin J. Change in failure stress on the southern San Andreas fault system caused by the 1992 Magnitude = 7.4 Landers earthquake. Science, Vol. 258, 1992, pp. 1328-1332, DOI:10/1126science.258.5086.1328.

Toda S., Stein R.S., Reasenberg P.A., Dieterich J.H., Yoshida A. Stress transferred by the 1995 Mw= 6.9 Kobe, Japan, shock: Effect on aftershocks and future earthquake probabilities. Journal of Geophysical Research: Solid Earth, Vol. 103, No. 10, 1998, pp. 24543-24565, DOI:org/10.1029/98J600765.

Toda S., Stein R.S., Richards-Dinger K., Bozkurt S.B. Forecasting the evolution of seismicity in southern California: Animations built on earthquake stress transfer. Journal of Geophysical Research: Solid Earth, Vol. 110, No. 5, 2005, 17 p., DOI: 10.1029/2004JBOO3415.

Tregoning P., McQueen H., Lambeck K., Jackson R., Little R., Saunders S., Rosa R., Present-day crustal motion in Papua New Guinea. Earth, planets and space, Vol. 52, No. 10, 2000, pp. 727-730.

Vavryčuk V. Iterative joint inversion for stress and fault orientations from focal mechanisms. Geophysical Journal International, Vol. 199, No. 1, 2014, pp. 69-77, DOI: org/1093/gji/ggu224.

Wallace L.M., Stevens C., Silver E., McCaffrey R., Loratung W., Hasiata S., Stanaway R., Curley R., Rosa R., Taugaloidi J. GPS and seismological constraints on active tectonics and arc-continent collision in Papua New Guinea: Implications for mechanics of microplate rotations in a plate boundary zone. Journal of Geophysical Research: Solid Earth, Vol. 109, No. 5, 2004, DOI: 10.1029/2003JBOO2481

Wells D.L., Coppersmith K.J. New empirical relationships among magnitude, rupture length, rupture width, rupture area, and surface displacement. Bulletin of the seismological Society of America, Vol. 84, 1994, pp. 974-1002, DOI:org/10.1785/BSSA0840040974.

Wessel P., Smith W.H., Scharroo R., Luis J., Wobbe F. The generic mapping tools: improved version released. EOS, Transactions American Geophysical Union, Vol. 94, No. 45, 2013, pp. 409-410, DOI: 10.1002/2013EO450001.

Prieta earthquake. Science, Vol. 255, No. 5052, 1992, pp. 1687-1690, DOI:10.1126/science 255.5052.1687.

Roeloffs E.A. Hydrologic precursors to earthquakes: A review. Pure and applied geophysics, Vol. 126, 1988, pp. 177-209.

Silver E.A., Moore J.C. The Molucca sea collision zone, Indonesia. Journal of Geophysical Research: Solid Earth, Vol. 83, 1978, pp. 1681-1691.

Simons W., van Loon D., Waspersdorf A., Ambrosius B., Kahar J., Abidin H., Sarsito D., Vigny C., Abu S.H., Morgan P. Geodynamics of SE Asia: First results of the Sulawesi 1998 GPS campaign. In: Geodesy Beyond 2000, Springer. 2000, pp. 271-277.

Socquet A., Simons W., Vigny C., McCaffrey R., Subarya C., Sarsito D., Ambrosius B., Spakman W. Microblock rotations and fault coupling in SE Asia triple junction (Sulawesi, Indonesia) from GPS and earthquake slip vector data. Journal of Geophysical Research: Solid Earth,Vol. 111, No. B8, 2006, DOI: org/10.1029JBOO3963.

Stevens C., McCaffrey R., Bock Y., Genrich J., Subarya C., Puntodewo S. and Vigny C. Rapid rotations about a vertical axis in a collisional setting revealed by the Palu fault, Sulawesi, Indonesia. Geophysical Research Letters, Vol. 26, No. 17, 1999, pp. 2677-2680, DOI:org/10.1029/1999GE008344.

Strader A.E. The effects of Coulomb stress change on Southern California earthquake forecasting. UCLA. ProQuest ID: Strader_ucla_0031D_12803. Merritt ID: ark:/13030/m58d22pj, 2014,166 , DOI:10.13140/RG.22.36576.48647.

Steacy S., Nalbant S.S., McCloskey J., Nostro C., Scotti O., Baumont D. Onto what planes should Coulomb stress perturbations be resolved? J. Geophys. Res., Vol. 110, No. B5, 2005, B05S15, DOI: 10.1029/2004JBOO3356.

Stein R.S., King G.C.P., Lin J. Change in failure stress on the southern San Andreas fault system caused by the 1992 Magnitude = 7.4 Landers earthquake. Science, Vol. 258, 1992, pp. 1328-1332, DOI:10/1126science.258.5086.1328.

Toda S., Stein R.S., Reasenberg P.A., Dieterich J.H., Yoshida A. Stress transferred by the 1995 Mw= 6.9 Kobe, Japan, shock: Effect on aftershocks and future earthquake probabilities. Journal of Geophysical Research: Solid Earth, Vol. 103, No. 10, 1998, pp. 24543-24565, DOI:org/10.1029/98J600765.

Toda S., Stein R.S., Richards-Dinger K., Bozkurt S.B. Forecasting the evolution of seismicity in southern California: Animations built on earthquake stress transfer. Journal of Geophysical Research: Solid Earth, Vol. 110, No. 5, 2005, 17 p., DOI: 10.1029/2004JBOO3415.

Tregoning P., McQueen H., Lambeck K., Jackson R., Little R., Saunders S., Rosa R., Present-day crustal motion in Papua New Guinea. Earth, planets and space, Vol. 52, No. 10, 2000, pp. 727-730.

Vavryčuk V. Iterative joint inversion for stress and fault orientations from focal mechanisms. Geophysical Journal International, Vol. 199, No. 1, 2014, pp. 69-77, DOI: org/1093/gji/ggu224.

Wallace L.M., Stevens C., Silver E., McCaffrey R., Loratung W., Hasiata S., Stanaway R., Curley R., Rosa R., Taugaloidi J. GPS and seismological constraints on active tectonics and arc-continent collision in Papua New Guinea: Implications for mechanics of microplate rotations in a plate boundary zone. Journal of Geophysical Research: Solid Earth, Vol. 109, No. 5, 2004, DOI: 10.1029/2003JBOO2481

Wells D.L., Coppersmith K.J. New empirical relationships among magnitude, rupture length, rupture width, rupture area, and surface displacement. Bulletin of the seismological Society of America, Vol. 84, 1994, pp. 974-1002, DOI:org/10.1785/BSSA0840040974.

Wessel P., Smith W.H., Scharroo R., Luis J., Wobbe F. The generic mapping tools: improved version released. EOS, Transactions American Geophysical Union, Vol. 94, No. 45, 2013, pp. 409-410, DOI: 10.1002/2013EO450001.

Walpersdorf A., Rangin C., Vigny C. GPS compared to long-term geologic motion of the north arm of Sulawesi. Earth and Planetary Science Letters, Vol. 159, 1998, pp. 47-55.

Walpersdorf A., Rangin C., Vigny C. GPS compared to long-term geologic motion of the north arm of Sulawesi. Earth and Planetary Science Letters, Vol. 159, 1998, pp. 47-55.

ВЛИЯНИЕ ИЗМЕНЕНИЙ КУЛОНОВСКОГО НАПРЯЖЕНИЯ ПРИ ЗЕМЛЕТРЯСЕНИИ СИЛОЙ M_W =7.5 В ПАЛУ, ИНДОНЕЗИЯ В 2018 г.

Ахадов Б.[1,2], Чин Ш.[3,4]

[1]Министерство науки и образования Азербайджанской Республики, Институт геологии и геофизики
AZ1143, Баку, просп. Г.Джавида, 119: (ahadovshao@gmail.com)
[2]Министерство науки и образования Азербайджанской Республики, Институт нефти и газа, Азербайджан
AZ1000, Баку, ул. Ф.Амирова, 9
[3]Шанхайская астрономическая обсерватория, Китайская академия наук,
80 Нандан роуд, Шанхай 200030, Китай
[4]Школа геодезии и земельной информатики, Хэнаньский политехнический университет,
Цзяоцзо 454000, Китай

Резюме. В данной статье представлены результаты изучения влияния кулоновского напряжения для выяснения процесса разрушения системы разломов Палу-Коро. 28 сентября 2018 г. на крупном сдвиговом разломе в северной части острова Сулавеси, Индонезия, произошло землетрясение. В результате кулоновское напряжение увеличилось примерно на 1 бар в областях афтершоков и областях, где напряжение уменьшилось более чем на 10 бар. На основе фокальных механизмов афтершоков и моделей очагов главного толчка рассчитаны изменения кулоновского напряжения разрушения на обеих узловых плоскостях фокального механизма. Дополнительно были рассчитаны изменения кулоновского напряжения в очагах каждого афтершока. Представленная нами модель напряжений указывает на положительную корреляцию между расширенными кулоновскими полями напряжений, возникающими в результате сочетания сейсмической активности. Нами было исследовано кулоновское напряжение как возможный источник афтершоков, которые имеют тенденцию оптимально смещаться ввиду разрушения из-за локального поля напряжений, созданного основным толчком. Землетрясение силой 7.5 баллов, происшедшее в Палу, привело к распределению смещений поверхности. Кроме того, расчетное горизонтальное смещение варьрует от 1 до 1.3 метра в направлении СЗ-ЮЗ. Карты напряжений, включенные в эту статью, имеют большое значение для прогнозирования ожидаемых мест будущих толчков и снижения последствий землетрясений. Было подтверждено, что оценка кулоновского напряжения, связанного со смещением землетрясения, является важным средством понимания различных сейсмических явлений.

Ключевые слова*: кулоновское напряжение, инверсия напряжений, деформация, землетрясение, Палу, Индонезия*

2018 M_W = 7.5 PALU, İNDONEZİYA, ZƏLZƏLƏSİNİN COULOMB STRESS DƏYİŞİKLİKLƏRİNİN TƏSİRİ

Əhədov B.[1,2], Çin Ş.[3,4]

[1]Azərbaycan Respublikası Elm və Təhsil Nazirliyi, Geologiya və Geofizika Institutu
AZ1143, Bakı, G.Cavid prospekti, 119: ahadovshao@gmail.com
[2]Azərbaycan Respublikası Elm və Təhsil Nazirliyi, Neft və Qaz İnstitutu, Azərbaycan
AZ 1000, Bakı şəh., F. Əmirov küç., 9
[3]Şanxay Astronomiya Rəsədxanası, Çin Elmlər Akademiyası, Çin
80 Nandan Road, Şanxay 200030, Çin
[4]Henan Politexnik Universiteti, Geodeziya və Torpaq İnformasiya Mühəndisliyi Məktəbi
Jiaozuo 454000, Çin

Xülasə. Bu məqalədə Palu-Koro qırılma sistemində qırılma prosesini anlamaq üçün Coulomb gərginliyinin təsirləri araşdırılmışdır. 2018-ci il sentyabrın 28-də İndoneziyanın şimalındakı Sulavesi adasında böyük qırılıb-sürüşmə mexanizmli zəlzələ baş vermişdir. Nəticədə Coulomb (Kulon) gərginliyi təxminən 1 bar artmış və bu afterşokların paylandığı ərazilər ilə eyni zamanda gərginliyin 10 bardan çox aşağı düşdüyü ərazilərə aid olmuşdur. Məqalədə hər bir afterşok təkanların fokal mexanizmlərinə və əsas təkan mexanizm modellərinə əsasən, hər bir fokal mexanizmin hər iki nodal müstəvilərində Coulomb gərginliyinin dəyişməsi hesablanmışdır. Bundan əlavə afterşokların fokal mənbələrində Coulomb gərginlik dəyişiklikləri də hesablanmışdır. Əsas təkanın yaratdığı lokal gərginlik sahəsinə görə qırılma üçün optimal yerdəyişməyə meyilli olan afterşok təkanlarının mümkün mənbəyi kimi Coulomb gərginliyi araşdırılmışdır. Bizim gərginlik modelimiz seysmik aktivliyin təsirindən yaranan genişləndirilmiş Coulomb gərginlik bölgələri ilə müsbət korrelyasiya olduğunu göstərir. Palu 7.5 zəlzələsi yer səthində yerdəyişmələrə səbəb olmuşdur. Bundan başqa, hesablamalar üfüqi yerdəyişmənin Şimal-Qərb və Cənub-Qərb istiqamətində olduğunu və 1-1.3 metr arasında dəyişdiyini döstərmişdir. Palu zəlzələsinin Palu-Koro qırılmasının bitişik seqmentinə ötürdüyü gərginlik gərginliyi 1-2 bara çatma istiqamətində yükləyirdi. Gərginliyin modelləşdirilməsi təsdiq edir ki, kiçik artım (bir neçə bar) zəlzələlərin yaranmasına təkan verə bilər. Bu məqalədə göstərilən gərginlik xəritələri, gələcəkdəki afterşokların gözlənilən yerlərini proqnozlaşdırmaq və zəlzələ riskini azaltmaq üçün əhəmiyyətlidir.

Açar sözlər*: Coulomb stres, stres inversiyası, deformasiya, zəlzələ, Palu, Indoneziya*